THE JOURNAL OF PHYSICAL CHEMISTRY C
A JOURNAL OF THE AMERICAN CHEMICAL SOCIETY

pubs.acs.org/JPCC Article

Imaging of Nanoscale Gold in "Intact" Biological Cells by Environmental Electron Microscopy

Published as part of The Journal of Physical Chemistry virtual special issue "Marie-Paule Pileni Festschrift".

Domagoj Belić,* Oihane Fragueiro, Dina Salah, Alison Beckett, Martin Volk, and Mathias Brust*

Cite This: https://doi.org/10.1021/acs.jpcc.1c09104 Read Online

ACCESS | Metrics & More | Article Recommendations | Supporting Information

ABSTRACT: The ability to monitor the cellular uptake and distribution of engineered nanomaterials is a basic requirement in nanomedicine and nanotoxicology. This is commonly achieved by using optical and electron microscopies. Optical microscopy allows for easy sample preparation and live cell imaging but is inherently limited in resolution to typically hundreds of nanometers, making it unsuitable for detailed investigation of nanoscale objects. On the other hand, electron microscopy allows for imaging with subnanometer resolution but requires a dedicated sample preparation that is usually destructive and can be cumbersome and costly. Here we demonstrate direct imaging of engineered nanomaterials in biological cells under preservation of cellular ultrastructure by means of environmental scanning electron microscopy (ESEM) and wet scanning transmission electron microscopy (wet-STEM). Specifically, we outline protocols for imaging fully hydrated cells on glass slides or TEM grids, requiring no prior processing steps. This enables high-throughput analysis of structurally uncompromised biological samples with nanometer resolution by using a minimal electron dose (<1 $e^-/Å^2$) at low electron energy (≤30 keV). Here we refer to these cells as "intact", which should not be interpreted as "alive", although the cells are alive before being exposed to the electron beam. Our approach can be a viable alternative to the established electron microscopy methods for cellular imaging.

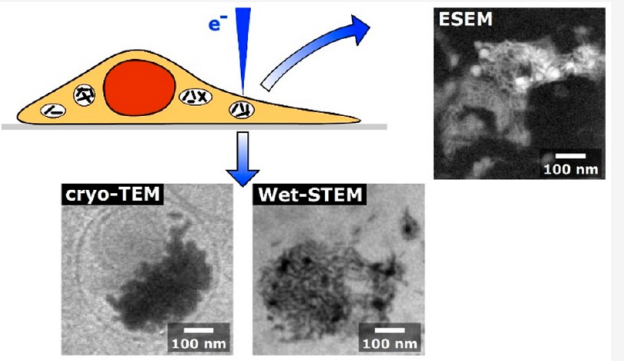

INTRODUCTION

In recent years, we have witnessed remarkable developments in the field of engineered nanomaterials (ENMs), including prospects of successfully interfacing biomedicine with materials science.[1] Nanoparticle−biostructure hybrid systems are of great interest for *in vitro* and *in vivo* biomedical applications.[2,3] Ordered ensembles of nanoparticles with emerging collective properties are also beginning to play a role in the biomedical sciences.[4,5] In particular, nanoscale gold has long been a focal point in biomedical research due to its high contrast, chemical stability, low toxicity, and ease of production.[6−10] Furthermore, gold nanoparticles can easily be functionalized with biocompatible ligands that can facilitate their uptake into living cells by endocytosis.[11−18] Once present inside the cells or surrounding tissue, nanoscale gold can serve a variety of purposes including diagnostics, drug delivery, cell tracking, DNA tagging, photothermal and photodynamic therapy, radiation dose enhancement, and advanced surgery.[19−37]

Alongside the many predicted beneficial applications of ENMs, there is also a growing concern about potential negative impacts of ENMs present in our environment.[38−40] The ability to quickly and accurately acquire direct visual information about the fate of nanomaterials taken up by cells and tissues is thus highly desirable. Traditionally, biological materials have been observed by noninvasive optical microscopy. This approach is still the standard method for their examination, anywhere from hospitals to research laboratories. However, the fundamental diffraction limit of light microscopy prevents detailed optical observations with nanometer resolution. Newly developed optical super-resolution techniques have managed to surpass this theoretical limitation, but their resolution is still on the order of tens of nanometers,[41] which is often insufficient for the detailed imaging of intracellular ENMs. On the other hand, electron microscopy (EM) is a proven technique routinely used for the investigation of nanoscale objects, allowing for detailed structural and chemical information at a subnanometer level. Because conventional EM requires analysis of specimens in high vacuum, hydrated biological materials are not suitable for direct imaging.

Received: October 20, 2021
Revised: November 26, 2021

To overcome this drawback, two methodological approaches are commonly used when dealing with EM of biomaterials: preparation of samples by fixation−staining−embedding−sectioning protocols for conventional EM[42] or vitrification of samples for cryo-electron microscopy (cryo-TEM).[43] In addition, over the past few years, a couple of more sophisticated imaging methods—correlative light-electron microscopy (CLEM) and liquid-cell electron microscopy (LCEM)—have emerged as a very appealing approach for studying nanoscale objects in cells with improved resolution.[44−50] What is more, LCEM allows for direct imaging of specimens in aqueous environments, including hydrated biological samples, placed within either a special silicon nitride cell or graphene enclosure.[51−65] In all these cases, though, significant amounts of time and resources as well as a range of specific skills and instrumentation are needed to successfully prepare and analyze the samples.

If possible, simpler and less onerous methods are therefore wanted. From that perspective, recently developed atmosphere scanning electron microscopy (ASEM) represents an important step in this direction: hydrated fixed cells can be imaged at 5 nm resolution in an inverted SEM via a thin silicon nitride window.[66,67] Based on ASEM, scanning electron-assisted dielectric microscopy (SE-ADM) was developed to image hydrated nonfixed cells with negligible radiation damage at 8 nm resolution.[68−70] In another version of ASEM, the microscope column is isolated by a bilayer graphene window, improving the resolution down to 5 nm.[71]

While these techniques allow for imaging of specimens in an open atmosphere, with little or no sample preparation involved, the use of windows seems to limit the achievable resolution. Environmental electron microscopy, on the other hand, can combine the favorable characteristics of atmospheric EM (minimal or no sample preparation) with conventional EM (high spatial resolution). In environmental EM, hydrated samples can be placed directly into an environmental scanning electron microscope operating in a pressure range between a few hundred and a few thousand pascal, in an atmosphere of 100% relative humidity.[72,73] It is worth noting that no silicon nitride window/cell nor graphene cover is necessary for successful imaging. Two complementary modes of environmental EM can be used: environmental scanning electron microscopy (ESEM), in which the secondary electrons ejected from the sample are collected on a detector above the sample via cascade amplification with gas molecules,[74] and wet scanning transmission electron microscopy (wet-STEM; sometimes also termed STEM-in-SEM), in which the transmitted primary electrons are collected by a STEM detector located below the sample.[75−77] This EM technique enables *in situ* investigation not only of metallic samples, such as gold nanoparticles and nanorods during wetting and drying,[78−81] but also of nonconductive samples, such as wet hybrid nanoparticles,[82] block copolymer vesicles,[83] latex beads,[84,85] water−oil emulsions,[86] and, more importantly, fixed and nonfixed biological samples.[87−102] Some of these studies included incubation of mammalian cells with nanogold serving as a label for specific cell membrane-based biomolecules, allowing for tracking their positions on the cell surface. It should also be noted that fixation protocols themselves might cause translocation of biomolecules across cellular compartments, so ideally fixation should be completely avoided.[103] However, until now, direct nanoscale environmental EM imaging of ENMs that are distributed within nonfixed intact cells in the absence of cover or enclosure has been elusive.

We here demonstrate the feasibility of environmental EM to image ENMs inside intact mammalian cells, without any further processing steps or use of any enclosure. Utilizing gold nanorods (GNRs) as a model ENM, we experimentally investigated their uptake into mesenchymal stem cells (MSCD1) by a means of ESEM and wet-STEM. Building upon the established ESEM practices,[72,104−108] we have developed new ESEM and wet-STEM protocols suitable for observing nanoscale gold in intact biological cells in a fully hydrated state, in a typical modern environmental electron microscope (FEI Quanta 250 FEG-ESEM). We show that electron doses on the order of 1 $e^-/Å^2$ are sufficient for capturing fine details on the nanoscale. To corroborate the accuracy of our ESEM and wet-STEM observations, we have also imaged equivalent samples prepared by conventional biological EM techniques, that is, fixation−staining−embedding−sectioning TEM, or cryo-TEM. All the results are compared, highlighting the innovative aspects of ESEM and wet-STEM with respect to common EM approaches when dealing with the analysis of ENMs present inside cells.

EXPERIMENTAL METHODS

Reagents. All chemicals were of highest available purity, purchased from Sigma-Aldrich, Prochimia, and LifeTein, and used as received. All solutions were prepared with deionized (Milli-Q) water.

Preparation of GNRs. GNRs were prepared following the well-established seeded growth method reported by Nikoobakht and El-Sayed.[109] Typically, the seed solution was obtained by mixing 2.5 mL of $HAuCl_4$ (1 mM) with 5 mL of CTAB (200 mM) and then adding 60 μL of an ice-cooled $NaBH_4$ (100 mM). The mixture was left to rest for 2 h. Then, 16 μL of this seed solution was added under stirring to the growth solution consisting of a mixture of 10 mL of $HAuCl_4$ (1 mM), 10 mL of CTAB (200 mM), 500 μL of $AgNO_3$ (4 mM), and 140 μL of ascorbic acid (78.8 mM). The reaction mixture was kept at rest overnight at 27 °C and then used as stock solution for further experiments.

Surface Modification of GNRs. To remove excess CTAB, the GNR stock solution was centrifuged twice (14500 rpm, 20 min), and the GNRs were resuspended in Milli-Q water each time. A carefully dosed amount of poly(ethylene glycol) monomethyl ether thiol ($HS-(CH_2)_2-O-(EG)_n-CH_3$) of 5000 g mol^{-1} average molecular weight (PEG_{5000}) was added to retain good stability of the GNRs but avoid saturation of all available surface sites with thiolate bonds. To achieve this, depending on the amount of GNR stock solution used, the conditions were chosen so that ∼100000 PEG_{5000} molecules were available for each GNR. Then, the modified cell penetrating peptide CALNN-TAT (LifeTein) was added (∼3000 molecules per GNR) and again left overnight to react. Before use, the suspension was purified by centrifugation.

Negative Staining of GNRs for TEM. 4 μL of GNR solution was dropcast onto a freshly glow-discharged (Quorum Q150T) carbon-coated TEM grid, gently blotted with filter paper, and then consecutively immersed in two 20 μL drops of 1.5% uranyl acetate (UA) solution for 30 s. The excess liquid was gently removed by using a filter paper and let to completely dry in a fume hood before TEM imaging.

UV−Vis−NIR. UV−vis−NIR spectroscopy was conducted in a Thermo Scientific Genesys 10S UV−vis spectrometer.

https://doi.org/10.1021/acs.jpcc.1c09104
J. Phys. Chem. C XXXX, XXX, XXX−XXX

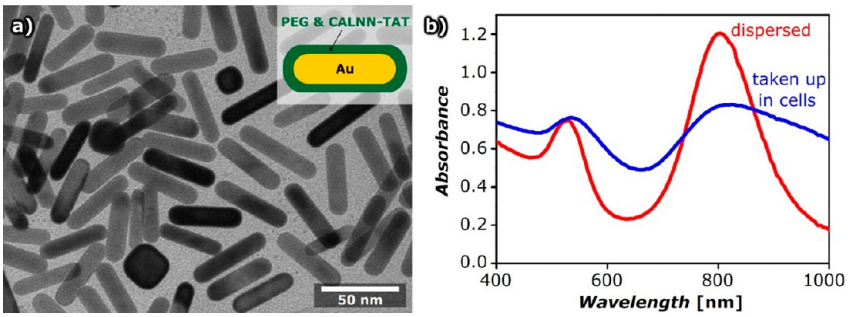

Figure 1. (a) TEM image of GNRs functionalized with thiolated PEG and CALNN-TAT.(b) UV−vis−NIR spectra of GNRs dispersed in solution and taken up in MSCD1 cells. The peak broadening and shift observed upon cellular uptake is reversible after cell lysis, supporting our interpretation that it is due to plasmon coupling within densely packed endocytic vesicles.[28]

Cell Culture and Uptake of GNRs. Dulbecco's Modified Eagle Medium (DMEM) was obtained from Gibco. Phosphate-buffered saline (PBS) and penicillin−streptomycin were from Sigma-Aldrich. Fetal bovine serum (FBS) was purchased from Life Technologies.

Murine mesenchymal stem/stromal cells MSCD1 (CRL-12424) were used.[29] They were obtained from the bone marrow of the *Mus musculus* mouse (ATCC). In a typical uptake experiment, 2×10^5 MSCD1 cells were seeded in six-well plate with 2 mL cell culture medium (DMEM supplemented with 10% FBS) and incubated at 37 °C with 5% CO_2 humidified atmosphere for 24 h. After 24 h, the medium was replaced with 400 μL of GNR dispersion added to 1.6 mL of fresh medium with 1% penicillin−streptomycin. MSCs were incubated with GNRs for 24 h and imaged on a Leica optical microscope.

Sample Preparation UV−Vis−NIR Spectroscopy. After incubation with GNRs in a six-well microplate, the cells were washed several times with PBS buffer and dissociated by using trypsin. The cells were resuspended in fresh medium and washed twice with PBS buffer by sequential centrifugations (500*g* for 3 min), and the number of cells was determined by using an automated cell counter (TC10, BioRad). We transferred 9×10^5 cells in PBS buffer to Eppendorfs for UV−vis−NIR measurements.

ESEM and Wet-STEM Imaging. Here, we follow the guidelines for the recommended practices on minimum information reporting in bionano experimental literature (MIRIBEL).[110,111]

ESEM and wet-STEM experiments were done in a FEI Quanta 250 FEG-ESEM. Typically, a glass slide (for ESEM) or a TEM grid (for wet-STEM) containing labeled or control cells was taken from a 24-well plate and gently blotted with filter paper, ensuring that the surface remains visibly wet. The sample was then put onto a precooled stage and loaded into the ESEM for inspection. For experimental details on the pump-down procedure and imaging conditions see the Supporting Information. We note that each well in the 24-well plate contained up to four glass slides or TEM grids, allowing for a high number of experiments/attempts, only limited by the sample mounting/exchange procedure—usually up to 12 per standard day of work. In the case of a damaged sample or bad imaging conditions (e.g., due to overflooding or overdrying during the pump-down procedure), the sample was immediately taken out of the ESEM so that a new one could be inserted. In this way it was usually possible to achieve good outcome for 2−3 samples per day of work, yielding useful data. In between the attempts, the 24-well plate was placed back into the incubator.

TEM Imaging. The samples were prepared for transmission electron microscopy (TEM) using the following protocol: after 24 h incubation, cells were fixed with a solution containing 1% paraformaldehyde and 3% glutaraldehyde in 0.1 M cacodylate buffer (pH 7.4). Then, cells were incubated with a reduced osmium staining solution, containing 2% OsO_4 and 1.5% $K_4[Fe(CN)_6]$, for 1 h. This was followed by a second 1 h osmium staining (2% OsO_4) step and overnight staining with 1% uranyl acetate. Cells were washed with water for 3 min, three times after every staining step. Samples were then dehydrated in graded ethanol (30%, 50%, 70%, 90%, and $2 \times$ 100%) for 5 min each. Finally, samples were infiltrated with medium TAAB resin 812 and embedded within the same resin. The resin was cured for 48 h at 60 °C. Finally, ultrathin sections of 350 μm × 350 μm × 74 nm were cut on a Leica UC6 microtome and placed on 200-mesh formvar/carbon TEM grids. They were poststained with uranyl acetate (4% UA in a 50:50 ethanol/water solution) and Reynolds lead citrate before TEM imaging.

The samples were imaged on a FEI Tecnai G2 Spirit BioTwin TEM operating at an accelerating voltage of 120 kV by using a SIS MegaView III digital camera.

Cryo-TEM Imaging. For cryo-TEM, the samples were prepared in the following way: cells were grown directly on carbon-coated gold TEM grids (Agar Scientific) in 24-well plates, as described earlier. Typically, a TEM grid with the GNR-labeled cells was taken from the well and put straight into a FEI Vitrobot Mk2 vitrification system operating at 8 °C and a relative humidity of >95%. The grid was blotted 2×2 s before being plunged into liquid ethane. The vitrified samples were stored in liquid nitrogen until examination. Cryo-TEM imaging was done on a FEI Tecnai G2 Spirit BioTwin TEM at 120 kV in low-dose conditions. During cryo-TEM, the sample holder (Gatan 626) was kept at a temperature below −178 °C.

Image Processing. All microscopy images were processed in Fiji/ImageJ. For visualization improvement, some of the ESEM and wet-STEM images were Gaussian-filtered or smoothed to reduce noise. In addition, these images were contrast/brightness adjusted during application of Green Fire Blue LUT.

RESULTS AND DISCUSSION

For this study, we have imaged gold nanorods (GNRs) that had been endocytosed by mesenchymal stem cells. The GNRs were coated with a mixed monolayer consisting predominantly of thiolated poly(ethylene glycol) (PEG) and a small amount

https://doi.org/10.1021/acs.jpcc.1c09104
J. Phys. Chem. C XXXX, XXX, XXX−XXX

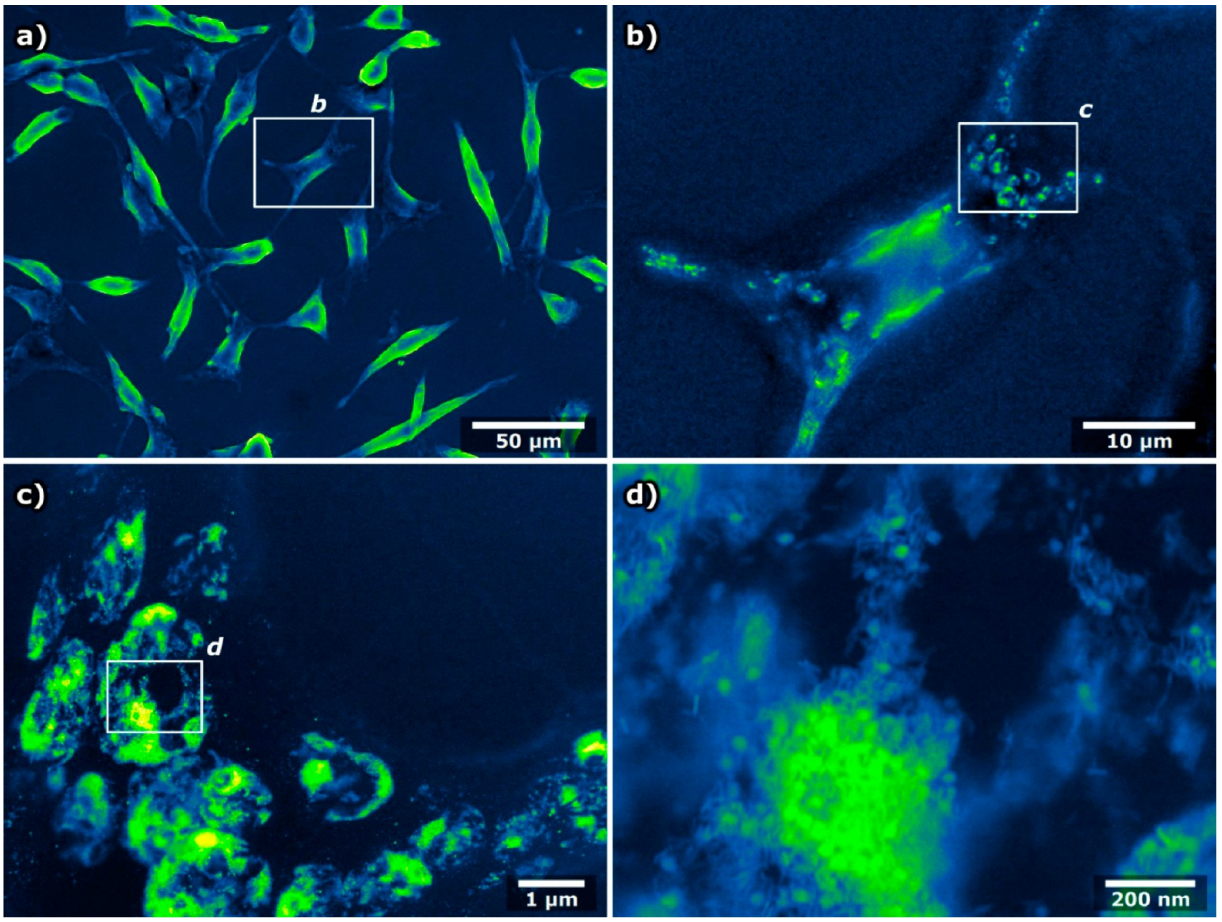

Figure 2. ESEM images (false colored) of fixed hydrated MSCD1 cells incubated with GNRs. The rectangles shown on the images indicate the successive zoomed-in areas. Electron doses for individual image acquisition were as follows: (a) 0.0016 $e^-/Å^2$, (b) 0.04 $e^-/Å^2$, (c) 1.44 $e^-/Å^2$, and (d) 16 $e^-/Å^2$.

of the cell-penetrating peptide TAT[13,14,112] appended to the pentapeptide CALNN, which is known to strongly bind to the surface of gold nanoparticles[113] (Figure 1a and Figure S1). The GNRs were readily incorporated by the cells as initially evidenced by optical microscopy (Figure S2). Uptake was also assessed by optical spectroscopy of suspensions of GNRs and of cells containing GNRs (Figure 1b). Both the transversal and the longitudinal peaks characteristic of GNRs were significantly broadened and slightly red-shifted when the GNRs were internalized within the cells indicating plasmon coupling, previously reported to be due to the compacting of the GNRs within endocytic vesicles.[28] This was reversible when the GNRs were released from the cells.

ESEM Imaging. Environmental electron microscopy was explored as a means to investigate the distribution of GNRs within cells. The experimental protocol for ESEM was initially developed and optimized by using fixed cells (Figures S3 and S4). Fixation makes the cells more robust for ESEM, allowing for longer examination of the sample while varying parameters such as temperature, pressure, humidity, electron beam energy, acquisition mode, dwell time, magnification/pitch, and working distance. Figure 2 shows hydrated fixed cells imaged by ESEM using a beam energy of 20 keV, where the brighter areas seen within the cells indicate incorporation of GNRs in endocytic vesicles (Figure 2b,c). At a higher magnification, individual GNRs can be clearly distinguished at nanometer resolution (Figure 2d), demonstrating that ESEM can be used for direct imaging of nanomaterials inside hydrated biological systems. It should be mentioned that at high magnification the electron flux might become sufficiently intense to immediately cause visible physical damage to biological material.[96,114−119] We took special care to minimize these undesired effects by keeping the electron beam dose adequately low (8−33 $e^-/Å^2$, at the highest tested nominal magnification of 100000×; see the Supporting Information for details), while still aiming to acquire images of the best possible clarity and resolution. Once optimized, the experimental procedure was repeated with excellent reproducibility, allowing for straightforward visual distinction between the cells that contained GNRs and the control sample comprising cells without GNRs (Figure S5).

In the next step, the goal was to directly image GNRs in nonprocessed intact live cells by using ESEM. To maintain the atmosphere around the sample inside the microscope close to a relative humidity of 100%, the sample holder was kept at a temperature of 2 °C.

The typical electron doses used in our high-resolution experiments (8−33 $e^-/Å^2$) are likely to cause cell death during imaging, although the lethal electron doses for cells are still subject to debate.[120−122] Therefore, the term "live" describes the state of the cells just prior to their insertion into the environmental microscope. By carefully setting the ESEM parameters (Figure S4), it was possible to achieve very slow evaporation of samples inside the microscope, so that the cells were kept hydrated in the leftover original buffer solution. This

https://doi.org/10.1021/acs.jpcc.1c09104
J. Phys. Chem. C XXXX, XXX, XXX−XXX

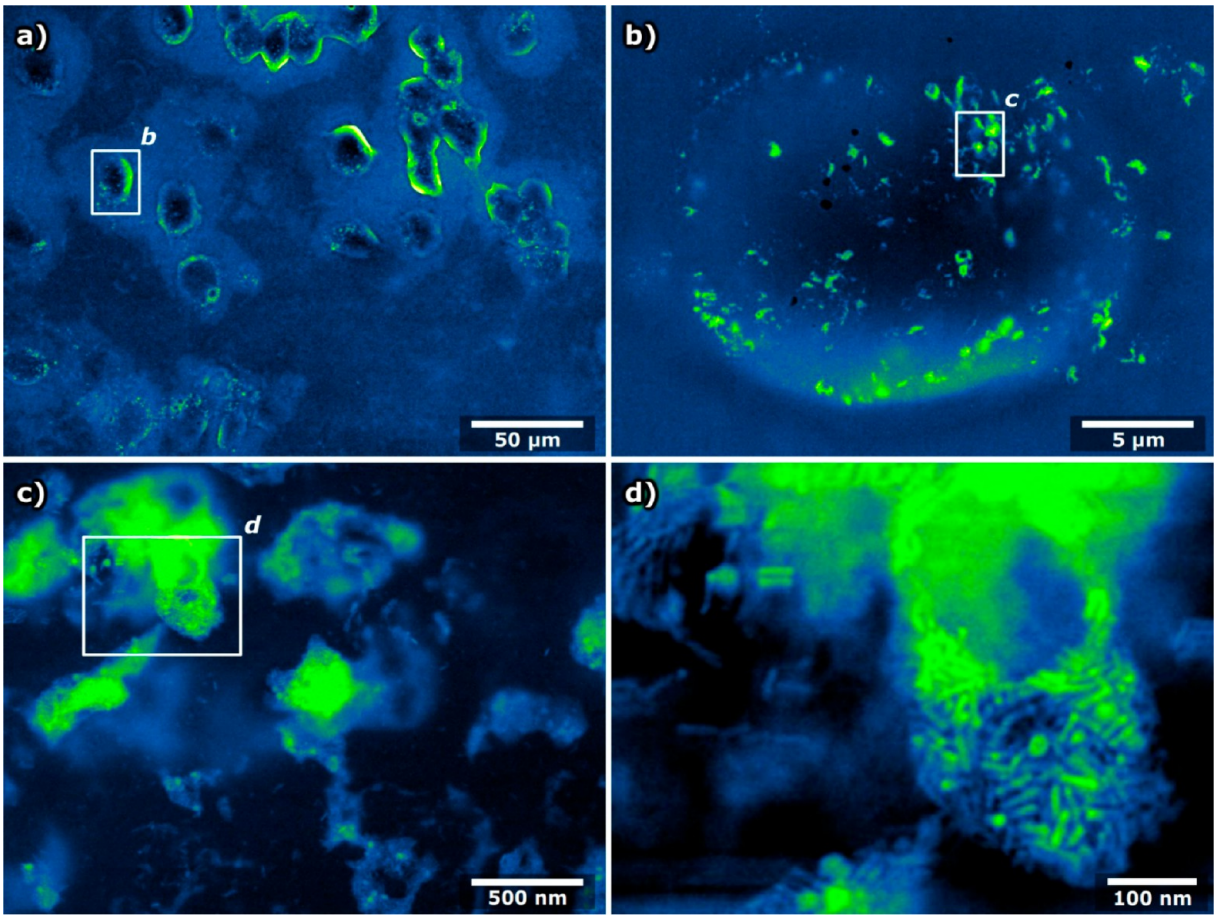

Figure 3. ESEM images (false colored) of intact, fully hydrated MSCD1 cells incubated with GNRs. The rectangles shown on the images indicate the successive zoomed-in areas. Electron doses during image acquisition were as follows: (a) 0.0033 $e^-/Å^2$, (b) 0.33 $e^-/Å^2$, and (c, d) 33 $e^-/Å^2$. Note that the cells are partially immersed in buffer solution.

enabled detailed imaging of the intact hydrated cells, as depicted in Figure 3. Again, the presence of the GNRs was evidenced by brighter regions or pockets within the cells, indicative of their confinement in endocytic vesicles (Figure 3b,c). At sufficiently high magnifications, individual GNRs close to the surface of these pockets are clearly resolved (Figure 3d). These cells appeared to be somewhat more prone to damage at higher electron beam doses (>10 $e^-/Å^2$) than the fixed cells. The pockets of GNRs tended to drift during image acquisition at higher magnifications (>50000×), visibly affecting the shape of the cell and leaving behind indentation-like rectangular features that corresponded to the imaged areas (not shown). Interestingly, this did not lead to detectable cell lysis. In comparison, ESEM images of the control samples (without GNRs) showed no signs of brighter pockets (Figure S6). This demonstrates that ESEM imaging at a magnification as low as 5000× is sufficient to make a clear distinction between cells that contain GNRs and those that do not. In addition, it appears feasible to estimate the extent of cellular uptake from the number, density, and relative brightness of these pockets within the cells, and in some cases, conclusions on the spatial distribution of ENMs (e.g., whether they are membrane-bound or taken up within cytoplasm) may be drawn, even at such low magnification. We note that these images were obtained with electron beam doses on the order of 0.01 $e^-/Å^2$, which is orders of magnitude lower than the doses typically used in cryo-TEM and potentially below the critical doses for survival of biological samples.[47,120,122] It is also worth noting that the electron beam energy used in our ESEM experiments (20 keV) was by an order of magnitude less than what is typically used in LCEM or cryo-TEM (200 keV).

While aiming to maintain the slow evaporation conditions needed to image intact cells, condensation of water on the sample occasionally occurred (Figure S7). In such a case, the cell membranes burst due to osmotic flow of water into the cells, spilling out the cytosol, in which individual GNRs could clearly be identified. Whenever this occurred, it was typically prior to performing the first scan of the electron beam at low magnification (<1000×) and ultralow dose (<0.0016 $e^-/Å^2$), so that electron beam damage can be ruled out as the main cause of cell lysis.

Wet-STEM Imaging. We next employed wet-STEM to examine the cells in the scanning transmission mode using a beam energy of 30 keV. For this purpose, the cells were grown and incubated with GNRs directly on the amorphous carbon films of gold TEM grids, which enabled a quick transfer of samples to the environmental microscope. Such samples also lend themselves to immediate vitrification for complementary cryo-TEM observations. While the ESEM mode facilitates high-resolution imaging of intracellular GNRs that are close to the cell surface, the wet-STEM mode also enables imaging of GNRs deeper within the cytoplasm, provided the imaged area is thin enough for the electron beam to penetrate through.

https://doi.org/10.1021/acs.jpcc.1c09104
J. Phys. Chem. C XXXX, XXX, XXX−XXX

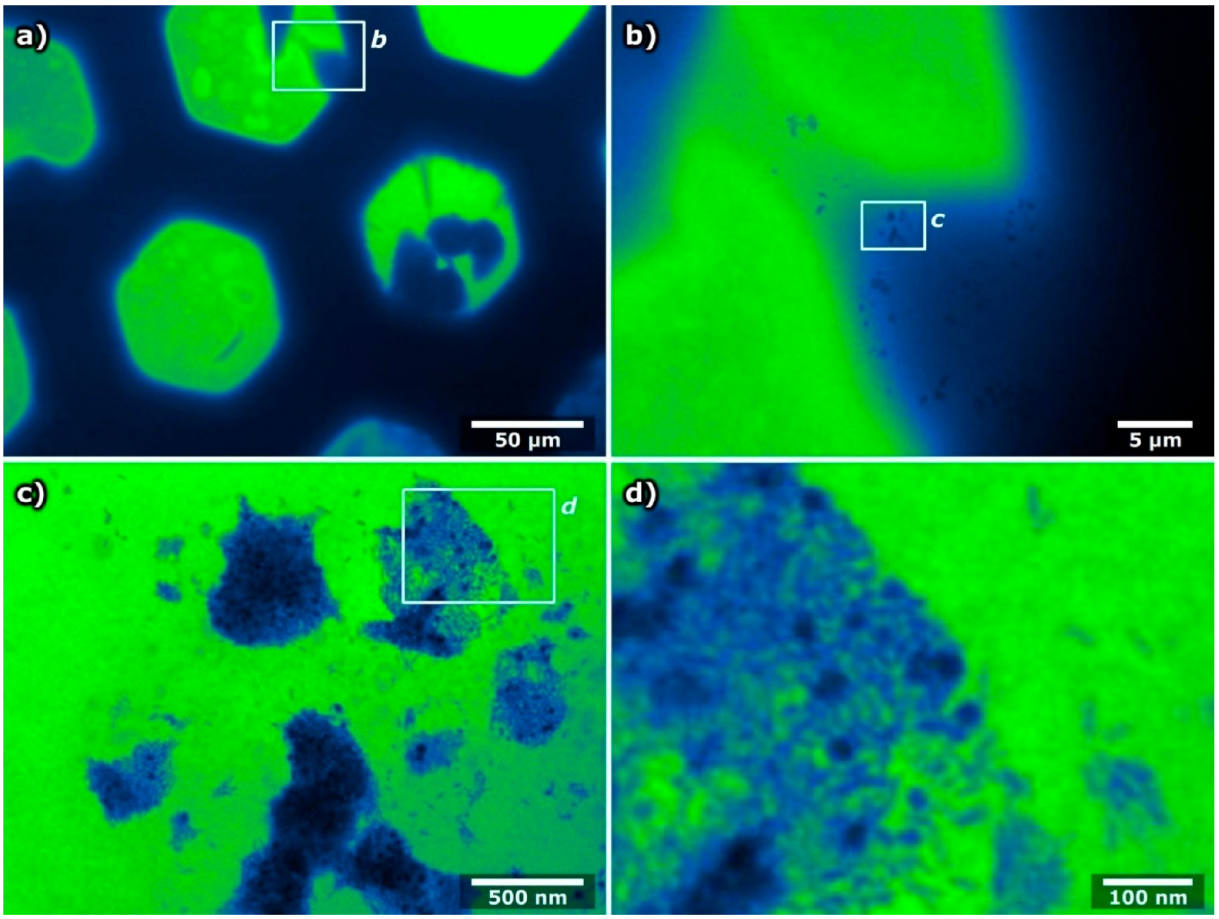

Figure 4. BF wet-STEM images (false colored) of intact, fully hydrated MSCD1 cells incubated with GNRs. The rectangles shown on the images indicate the zoomed-in areas (image d is digitally magnified). Electron doses for individual image acquisition were as follows: (a) 0.0016 $e^-/Å^2$, (b) 0.04 $e^-/Å^2$, and (c, d) 16 $e^-/Å^2$.

This represents an advantage of wet-STEM over ESEM, as it yields more accurate information about the distribution of nanomaterials within the cells. One should be careful though when interpreting wet-STEM micrographs because the profile of forward-scattered electrons is strongly influenced by geometric factors, such as sample thickness and the *z*-position of the nanomaterial contained.[123,124] For instance, one of the most obvious effects is contrast inversion,[84,125] so that GNRs could appear dark or bright on the same detector, depending on their exact position in the cell. On the other hand, the absence of silicon nitride windows in our wet-STEM experiments is beneficial for reducing the beam broadening and thus minimizing the image blurring.

To establish a working procedure for wet-STEM imaging of GNRs in cells, we followed the same line of experimentation as for ESEM. The imaging parameters were first adjusted by using fixed hydrated cells, serving as a good starting point for optimizing the protocol for imaging of untreated cells (Figures S8–S11). In comparison to ESEM, an additional benefit of wet-STEM experimental setup is a segmented solid-state STEM detector that can operate in both bright-field (BF) and dark-field (DF) modes at the same time, thus revealing more information from the scanned area (Figure S9).

Figure 4 shows wet-STEM images of a typical sample of intact cells containing GNRs. Initially fully hydrated and mostly covered by a layer of liquid buffer solution, the sample has a limited area that is suitable for observation in transmission mode (see also Figure S12). Slow evaporation of liquid within the environmental microscope rendered more area transparent enough to acquire wet-STEM images at higher resolution (Figure 4a). In the thinner parts of the cells (Figure 4b), darker features were resolved that corresponded in shape and size to the brighter pockets commonly observed in the respective ESEM images (Figure 3b).

A close-up wet-STEM view of these features (Figure 4c,d, Figures S13 and S14) reveals that they comprise locally tightly packed GNRs, in agreement with what was observed by ESEM. Such larger aggregates of GNRs are indicative of their confinement in endocytic vesicles. In addition, individual GNRs can be seen in places, at a resolution of a few nanometers; they appear to be at the same depth as the vesicles, i.e., located deep within the cytoplasm and not bound to the cell membrane. Again, control samples without GNRs did not show comparable features (Figure S13). Once optimized, our imaging protocol enabled routine screening of intact fully hydrated samples at a rate of up to a dozen per day.

Comparison with Thin-Section TEM and Cryo-TEM. To validate our ESEM and wet-STEM results against conventional methods, we made use of two EM approaches that are commonly utilized for imaging biomaterials, i.e., fixation–staining–embedding–sectioning of cells for standard TEM, and vitrification of cells for cryo-TEM. We stress that both techniques required significantly more time, materials,

https://doi.org/10.1021/acs.jpcc.1c09104
J. Phys. Chem. C XXXX, XXX, XXX–XXX

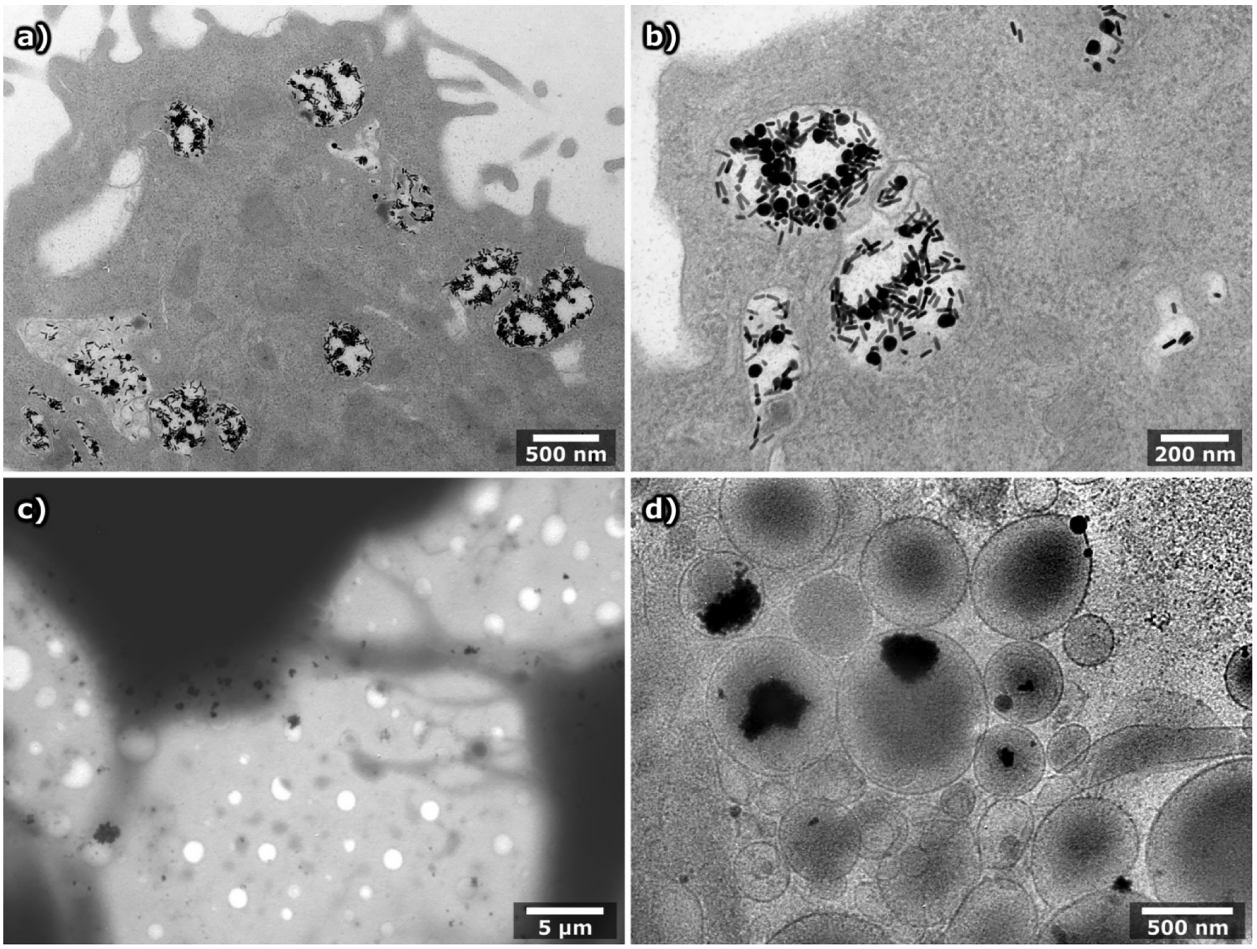

Figure 5. (a, b) TEM images of thin sections of MSCD1 cells incubated with GNRs. (c, d) Cryo-TEM images of whole vitrified MSCD1 cells incubated with GNRs. Electron doses during acquisition of cryo-TEM images in (c, d) were 6.3 and 31.8 $e^-/Å^2$, respectively. (Note: the presence of some spheres and irregularly shaped particles is a feature of the batch of nanorods used in this experiment. It is not due to beam damage or other later introduced modifications.)

instrumentation, and effort than the corresponding ESEM and wet-STEM experiments.

Figure 5a,b shows a couple of TEM images of thin sections sliced from cells incubated with GNRs. These images confirm that the GNRs are mostly confined and densely packed within endocytic vesicles. Only very few GNRs are found at or near the cell membrane as individual rods (see also Figure S15). This is in line with our ESEM and wet-STEM observations (Figures 2–4) as well as with the optical spectrum of the cells (Figure 1b) which indicates plasmon coupling due to close packing of GNRs.

Cryo-TEM images (Figure 5c and Figure S16) of vitrified whole cells that were grown directly on the TEM grid and incubated with GNRs exhibit features very similar to typical wet-STEM images (Figure 4b). A closer look at the thinner parts of the vitrified cells (Figure 5d) confirms that the GNRs are closely packed within vesicles.

The results obtained by using these two well-established EM techniques complement and support the conclusions drawn from our ESEM and wet-STEM observations. It seems that the quality of information that can be obtained by using relatively straightforward environmental EM techniques—ESEM and wet-STEM of nonprocessed cells—can match those obtained by using quite resource-demanding EM techniques. In addition, ESEM and wet-STEM experiments were performed by using an electron beam of a much lower energy (20 and 30 keV, respectively) than the one used in typical LCEM experiments (200 or 300 keV). Normally, lowering the beam energy leads to a loss of resolution in EM, but because ESEM and wet-STEM allow for direct observation of hydrated samples without any cover/enclosure, such as silicon nitride windows, and without a layer of excess liquid in between, the final ESEM and wet-STEM resolution (Figure S17) could match the resolution achieved in LCEM of samples of biological origin.

CONCLUSIONS

We have demonstrated the possibility to image nanomaterials within intact mammalian cells at a magnification as low as 5000×, i.e., electron beam doses on the order of 0.01 $e^-/Å^2$, by using a beam energy of 20 keV in ESEM mode or 30 keV in wet-STEM mode. While conventional TEM can provide more contrasted images, it was possible in both cases to clearly visualize GNRs within the cells with nanometer resolution by using doses on the order of 1 $e^-/Å^2$, either tightly packed in vesicles or as single particles. This opens up various possibilities, for instance to track nanogold-labeled biomolecules not only on the surface of the cellular membrane but also within the cytoplasm and within cellular compartments.

https://doi.org/10.1021/acs.jpcc.1c09104
J. Phys. Chem. C XXXX, XXX, XXX−XXX

In principle, environmental electron microscopy can be performed even at room temperature by using higher water vapor pressure, albeit at the expense of lower image resolution and clarity. In the next step, the imaging conditions should be tailored to ensure that the biological specimens remain alive during imaging. Hence, in spite of the many practical difficulties, we envisage the use of ESEM and wet-STEM for nanoscale imaging of living cellular matter and associated processes.

■ ASSOCIATED CONTENT

Supporting Information

The Supporting Information is available free of charge at https://pubs.acs.org/doi/10.1021/acs.jpcc.1c09104.

Additional negative-stain TEM images of GNRs, optical microscopy images of GNR-labeled cells, details on optimized experimental protocols for ESEM and wet-STEM imaging of fixed and intact (nonfixed) cells, additional ESEM and wet-STEM images of GNR-labeled and control samples, TEM images of thin sections, cryo-TEM images of vitrified GNR-labeled cells, wet-STEM resolution measurements and calculation of the electron dose used in our experiments (PDF)

■ AUTHOR INFORMATION

Corresponding Authors

Domagoj Belić − *Department of Chemistry, University of Liverpool, Liverpool L69 7ZD, United Kingdom; Department of Physics, Josip Juraj Strossmayer University of Osijek, 31000 Osijek, Croatia;* orcid.org/0000-0002-7954-7046; Email: Domagoj.Belic@liverpool.ac.uk

Mathias Brust − *Department of Chemistry, University of Liverpool, Liverpool L69 7ZD, United Kingdom;* orcid.org/0000-0001-6301-7123; Email: M.Brust@liverpool.ac.uk

Authors

Oihane Fragueiro − *Department of Chemistry, University of Liverpool, Liverpool L69 7ZD, United Kingdom*

Dina Salah − *Department of Chemistry, University of Liverpool, Liverpool L69 7ZD, United Kingdom; Biophysics Group, Physics Department, Ain Shams University, Cairo 11566, Egypt*

Alison Beckett − *Biomedical Electron Microscopy Facility, University of Liverpool, Liverpool L69 7ZB, United Kingdom*

Martin Volk − *Surface Science Research Centre, Department of Chemistry, University of Liverpool, Liverpool L69 3BX, United Kingdom*

Complete contact information is available at: https://pubs.acs.org/10.1021/acs.jpcc.1c09104

Author Contributions

M.B.: conceptualization, funding acquisition, resource, supervision, writing. D.B.: conceptualization, data acquisition, analysis, writing. O.F. and D.S.: sample preparation, data acquisition. A.B.: resources. M.V.: supervision.

Notes

The authors declare no competing financial interest.

■ ACKNOWLEDGMENTS

This research has received funding from the European Research Council under the European Union's Seventh Framework Programme (FP7/2007-2013)/ERC-Advanced Grant Project 321172 PANDORA. The authors thank Prof. Patricia Murray and Dr. Arthur Taylor for their advice and help with cell culture.

■ REFERENCES

(1) Björnmalm, M.; Faria, M.; Caruso, F. Increasing the Impact of Materials in and Beyond Bio-Nano Science. *J. Am. Chem. Soc.* **2016**, *138* (41), 13449−13456.

(2) Zhou, W.; Gao, X.; Liu, D.; Chen, X. Gold Nanoparticles for *in Vitro* Diagnostics. *Chem. Rev.* **2015**, *115* (19), 10575−10636.

(3) Smith, B. R.; Gambhir, S. S. Nanomaterials for *in Vivo* Imaging. *Chem. Rev.* **2017**, *117* (3), 901−986.

(4) Nicolas-Boluda, A.; Yang, Z.; Guilbert, T.; Fouassier, L.; Carn, F.; Gazeau, F.; Pileni, M. P. Self-Assemblies of Fe_3O_4 Nanocrystals: Toward Nanoscale Precision of Photothermal Effects in the Tumor Microenvironment. *Adv. Funct. Mater.* **2021**, *31* (4), 2006824.

(5) Nicolas-Boluda, A.; Yang, Z.; Dobryden, I.; Carn, F.; Winckelmans, N.; Péchoux, C.; Bonville, P.; Bals, S.; Claesson, P. M.; Gazeau, F.; et al. Intracellular Fate of Hydrophobic Nanocrystal Self-Assemblies in Tumor Cells. *Adv. Funct. Mater.* **2020**, *30* (40), 2004274.

(6) Boisselier, E.; Astruc, D. Gold Nanoparticles in Nanomedicine: Preparations, Imaging, Diagnostics, Therapies and Toxicity. *Chem. Soc. Rev.* **2009**, *38* (6), 1759−1782.

(7) Alkilany, A. M.; Nagaria, P. K.; Hexel, C. R.; Shaw, T. J.; Murphy, C. J.; Wyatt, M. D. Cellular Uptake and Cytotoxicity of Gold Nanorods: Molecular Origin of Cytotoxicity and Surface Effects. *Small* **2009**, *5* (6), 701−708.

(8) Connor, E. E.; Mwamuka, J.; Gole, A.; Murphy, C. J.; Wyatt, M. D. Gold Nanoparticles Are Taken Up by Human Cells but Do Not Cause Acute Cytotoxicity. *Small* **2005**, *1* (3), 325−327.

(9) Carnovale, C.; Bryant, G.; Shukla, R.; Bansal, V. Size, Shape and Surface Chemistry of Nano-Gold Dictate Its Cellular Interactions, Uptake and Toxicity. *Prog. Mater. Sci.* **2016**, *83*, 152−190.

(10) Dreaden, E. C.; Alkilany, A. M.; Huang, X.; Murphy, C. J.; El-Sayed, M. A. The Golden Age: Gold Nanoparticles for Biomedicine. *Chem. Soc. Rev.* **2012**, *41* (7), 2740−2779.

(11) Dykman, L. A.; Khlebtsov, N. G. Uptake of Engineered Gold Nanoparticles into Mammalian Cells. *Chem. Rev.* **2014**, *114* (2), 1258−1288.

(12) Yang, C.; Uertz, J.; Yohan, D.; Chithrani, B. D. Peptide Modified Gold Nanoparticles for Improved Cellular Uptake, Nuclear Transport, and Intracellular Retention. *Nanoscale* **2014**, *6* (20), 12026−12033.

(13) de la Fuente, J. M.; Berry, C. C. Tat Peptide as an Efficient Molecule To Translocate Gold Nanoparticles into the Cell Nucleus. *Bioconjugate Chem.* **2005**, *16* (5), 1176−1180.

(14) Krpetić, Ž.; Saleemi, S.; Prior, I. A.; Sée, V.; Qureshi, R.; Brust, M. Negotiation of Intracellular Membrane Barriers by TAT-Modified Gold Nanoparticles. *ACS Nano* **2011**, *5* (6), 5195−5201.

(15) Nativo, P.; Prior, I. A.; Brust, M. Uptake and Intracellular Fate of Surface-Modified Gold Nanoparticles. *ACS Nano* **2008**, *2* (8), 1639−1644.

(16) Oh, E.; Delehanty, J. B.; Sapsford, K. E.; Susumu, K.; Goswami, R.; Blanco-Canosa, J. B.; Dawson, P. E.; Granek, J.; Shoff, M.; Zhang, Q.; et al. Cellular Uptake and Fate of PEGylated Gold Nanoparticles Is Dependent on Both Cell-Penetration Peptides and Particle Size. *ACS Nano* **2011**, *5* (8), 6434−6448.

(17) Chithrani, B. D.; Chan, W. C. W. Elucidating the Mechanism of Cellular Uptake and Removal of Protein-Coated Gold Nanoparticles of Different Sizes and Shapes. *Nano Lett.* **2007**, *7* (6), 1542−1550.

(18) Chithrani, B. D.; Ghazani, A. A.; Chan, W. C. W. Determining the Size and Shape Dependence of Gold Nanoparticle Uptake into Mammalian Cells. *Nano Lett.* **2006**, *6* (4), 662−668.

(19) Dykman, L.; Khlebtsov, N. Gold Nanoparticles in Biomedical Applications: Recent Advances and Perspectives. *Chem. Soc. Rev.* **2012**, *41* (6), 2256−2282.
(20) Pelaz, B.; Alexiou, C.; Alvarez-Puebla, R. A.; Alves, F.; Andrews, A. M.; Ashraf, S.; Balogh, L. P.; Ballerini, L.; Bestetti, A.; Brendel, C.; et al. Diverse Applications of Nanomedicine. *ACS Nano* **2017**, *11* (3), 2313−2381.
(21) Chen, G.; Roy, I.; Yang, C.; Prasad, P. N. Nanochemistry and Nanomedicine for Nanoparticle-Based Diagnostics and Therapy. *Chem. Rev.* **2016**, *116* (5), 2826−2885.
(22) Wang, P.; Rahman, M. A.; Zhao, Z.; Weiss, K.; Zhang, C.; Chen, Z.; Hurwitz, S. J.; Chen, Z. G.; Shin, D. M.; Ke, Y. Visualization of the Cellular Uptake and Trafficking of DNA Origami Nanostructures in Cancer Cells. *J. Am. Chem. Soc.* **2018**, *140* (7), 2478−2484.
(23) Dreaden, E. C.; Mackey, M. A.; Huang, X.; Kang, B.; El-Sayed, M. A. Beating Cancer in Multiple Ways Using Nanogold. *Chem. Soc. Rev.* **2011**, *40* (7), 3391−3404.
(24) Alkilany, A. M.; Thompson, L. B.; Boulos, S. P.; Sisco, P. N.; Murphy, C. J. Gold Nanorods: Their Potential for Photothermal Therapeutics and Drug Delivery, Tempered by the Complexity of Their Biological Interactions. *Adv. Drug Delivery Rev.* **2012**, *64* (2), 190−199.
(25) Abdelrasoul, G. N.; Magrassi, R.; Dante, S.; d'Amora, M.; d'Abbusco, M. S.; Pellegrino, T.; Diaspro, A. PEGylated Gold Nanorods as Optical Trackers for Biomedical Applications: An *in Vivo* and *in Vitro* Comparative Study. *Nanotechnology* **2016**, *27* (25), 255101.
(26) Chadwick, S. J.; Salah, D.; Livesey, P. M.; Brust, M.; Volk, M. Singlet Oxygen Generation by Laser Irradiation of Gold Nanoparticles. *J. Phys. Chem. C* **2016**, *120* (19), 10647−10657.
(27) Huang, X.; El-Sayed, I. H.; Qian, W.; El-Sayed, M. A. Cancer Cell Imaging and Photothermal Therapy in the Near-Infrared Region by Using Gold Nanorods. *J. Am. Chem. Soc.* **2006**, *128* (6), 2115−2120.
(28) Comenge, J.; Fragueiro, O.; Sharkey, J.; Taylor, A.; Held, M.; Burton, N. C.; Park, B. K.; Wilm, B.; Murray, P.; Brust, M.; et al. Preventing Plasmon Coupling between Gold Nanorods Improves the Sensitivity of Photoacoustic Detection of Labeled Stem Cells *in Vivo*. *ACS Nano* **2016**, *10*, 7106.
(29) Comenge, J.; Sharkey, J.; Fragueiro, O.; Wilm, B.; Brust, M.; Murray, P.; Levy, R.; Plagge, A. Multimodal Cell Tracking from Systemic Administration to Tumour Growth by Combining Gold Nanorods and Reporter Genes. *eLife* **2018**, *7*, e33140.
(30) Meir, R.; Shamalov, K.; Betzer, O.; Motiei, M.; Horovitz-Fried, M.; Yehuda, R.; Popovtzer, A.; Popovtzer, R.; Cohen, C. J. Nanomedicine for Cancer Immunotherapy: Tracking Cancer-Specific T-Cells *in Vivo* with Gold Nanoparticles and CT Imaging. *ACS Nano* **2015**, *9* (6), 6363−6372.
(31) Zhu, X.-M.; Fang, C.; Jia, H.; Huang, Y.; Cheng, C. H. K.; Ko, C.-H.; Chen, Z.; Wang, J.; Wang, Y.-X. J. Cellular Uptake Behaviour, Photothermal Therapy Performance, and Cytotoxicity of Gold Nanorods with Various Coatings. *Nanoscale* **2014**, *6* (19), 11462−11472.
(32) Locatelli, E.; Monaco, I.; Comes Franchini, M. Surface Modifications of Gold Nanorods for Applications in Nanomedicine. *RSC Adv.* **2015**, *5* (28), 21681−21699.
(33) Choi, J.; Yang, J.; Bang, D.; Park, J.; Suh, J.-S.; Huh, Y.-M.; Haam, S. Targetable Gold Nanorods for Epithelial Cancer Therapy Guided by Near-IR Absorption Imaging. *Small* **2012**, *8* (5), 746−753.
(34) McMahon, S. J.; Hyland, W. B.; Muir, M. F.; Coulter, J. A.; Jain, S.; Butterworth, K. T.; Schettino, G.; Dickson, G. R.; Hounsell, A. R.; O'Sullivan, J. M.; Prise, K. M.; Hirst, D. G.; Currell, F. J. Biological Consequences of Nanoscale Energy Deposition near Irradiated Heavy Atom Nanoparticles. *Sci. Rep.* **2011**, *1* (1), 18.
(35) McQuaid, H. N.; Muir, M. F.; Taggart, L. E.; McMahon, S. J.; Coulter, J. A.; Hyland, W. B.; Jain, S.; Butterworth, K. T.; Schettino, G.; Prise, K. M.; Hirst, D. G.; Botchway, S. W.; Currell, F. J. Imaging and Radiation Effects of Gold Nanoparticles in Tumour Cells. *Sci. Rep.* **2016**, *6* (1), 19442.
(36) Jain, S.; Coulter, J. A.; Hounsell, A. R.; Butterworth, K. T.; McMahon, S. J.; Hyland, W. B.; Muir, M. F.; Dickson, G. R.; Prise, K. M.; Currell, F. J.; et al. Cell-Specific Radiosensitization by Gold Nanoparticles at Megavoltage Radiation Energies. *Int. J. Radiat. Oncol., Biol., Phys.* **2011**, *79* (2), 531−539.
(37) Malki, M.; Fleischer, S.; Shapira, A.; Dvir, T. Gold Nanorod-Based Engineered Cardiac Patch for Suture-Free Engraftment by Near IR. *Nano Lett.* **2018**, *18* (7), 4069−4073.
(38) Maynard, A. D.; Aitken, R. J.; Butz, T.; Colvin, V.; Donaldson, K.; Oberdorster, G.; Philbert, M. A.; Ryan, J.; Seaton, A.; Stone, V.; et al. Safe Handling of Nanotechnology. *Nature* **2006**, *444* (7117), 267−269.
(39) Maynard, A. D.; Aitken, R. J. 'Safe Handling of Nanotechnology' Ten Years On. *Nat. Nanotechnol.* **2016**, *11* (12), 998−1000.
(40) Wigger, H.; Kägi, R.; Wiesner, M.; Nowack, B. Exposure and Possible Risks of Engineered Nanomaterials in the Environment − Current Knowledge and Directions for the Future. *Rev. Geophys.* **2020**, *58* (4), e2020RG000710.
(41) Sigal, Y. M.; Zhou, R.; Zhuang, X. Visualizing and Discovering Cellular Structures with Super-Resolution Microscopy. *Science* **2018**, *361*, 880−887.
(42) Schrand, A. M.; Schlager, J. J.; Dai, L.; Hussain, S. M. Preparation of Cells for Assessing Ultrastructural Localization of Nanoparticles with Transmission Electron Microscopy. *Nat. Protoc.* **2010**, *5* (4), 744−757.
(43) Elbaum, M. Quantitative Cryo-Scanning Transmission Electron Microscopy of Biological Materials. *Adv. Mater.* **2018**, *30* (41), 1706681.
(44) de Boer, P.; Hoogenboom, J. P.; Giepmans, B. N. G. Correlated Light and Electron Microscopy: Ultrastructure Lights up! *Nat. Methods* **2015**, *12* (6), 503−513.
(45) Hoffman, D. P.; Shtengel, G.; Xu, C. S.; Campbell, K. R.; Freeman, M.; Wang, L.; Milkie, D. E.; Pasolli, H. A.; Iyer, N.; Bogovic, J. A.; et al. Correlative Three-dimensional Super-resolution and Block-face Electron Microscopy of Whole Vitreously Frozen Cells. *Science* **2020**, *367* (6475), eaaz5357.
(46) Wu, H.; Friedrich, H.; Patterson, J. P.; Sommerdijk, N. A. J. M.; Jonge, N. Liquid-Phase Electron Microscopy for Soft Matter Science and Biology. *Adv. Mater.* **2020**, *32* (25), 2001582.
(47) *Liquid Cell Electron Microscopy*; Ross, F. M., Ed.; Advances in Microscopy and Microanalysis; Cambridge University Press: Cambridge, 2016.
(48) De Yoreo, J. J.; Sommerdijk, N. A. J. M. Investigating Materials Formation with Liquid-Phase and Cryogenic TEM. *Nat. Rev. Mater.* **2016**, *1*, 16035.
(49) Ross, F. M. Opportunities and Challenges in Liquid Cell Electron Microscopy. *Science* **2015**, *350* (6267), aaa9886.
(50) de Jonge, N.; Ross, F. M. Electron Microscopy of Specimens in Liquid. *Nat. Nanotechnol.* **2011**, *6* (11), 695−704.
(51) Park, J.; Koo, K.; Noh, N.; Chang, J. H.; Cheong, J. Y.; Dae, K. S.; Park, J. S.; Ji, S.; Kim, I.-D.; Yuk, J. M. Graphene Liquid Cell Electron Microscopy: Progress, Applications, and Perspectives. *ACS Nano* **2021**, *15* (1), 288−308.
(52) Dunn, G.; Adiga, V. P.; Pham, T.; Bryant, C.; Horton-Bailey, D. J.; Belling, J. N.; LaFrance, B.; Jackson, J. A.; Barzegar, H. R.; Yuk, J. M.; et al. Graphene-Sealed Flow Cells for In Situ Transmission Electron Microscopy of Liquid Samples. *ACS Nano* **2020**, *14* (8), 9637−9643.
(53) Koo, K.; Dae, K. S.; Hahn, Y. K.; Yuk, J. M. Live Cell Electron Microscopy Using Graphene Veils. *Nano Lett.* **2020**, *20* (6), 4708−4713.
(54) Textor, M.; de Jonge, N. Strategies for Preparing Graphene Liquid Cells for Transmission Electron Microscopy. *Nano Lett.* **2018**, *18* (6), 3313−3321.

https://doi.org/10.1021/acs.jpcc.1c09104
J. Phys. Chem. C XXXX, XXX, XXX−XXX

(55) Smith, J. W.; Chen, Q. Liquid-Phase Electron Microscopy Imaging of Cellular and Biomolecular Systems. *J. Mater. Chem. B* **2020**, *8* (37), 8490−8506.
(56) Park, J.; Park, H.; Ercius, P.; Pegoraro, A. F.; Xu, C.; Kim, J. W.; Han, S. H.; Weitz, D. A. Direct Observation of Wet Biological Samples by Graphene Liquid Cell Transmission Electron Microscopy. *Nano Lett.* **2015**, *15* (7), 4737−4744.
(57) Wojcik, M.; Hauser, M.; Li, W.; Moon, S.; Xu, K. Graphene-Enabled Electron Microscopy and Correlated Super-Resolution Microscopy of Wet Cells. *Nat. Commun.* **2015**, *6*, 7384.
(58) Dahmke, I. N.; Verch, A.; Hermannsdörfer, J.; Peckys, D. B.; Weatherup, R. S.; Hofmann, S.; de Jonge, N. Graphene Liquid Enclosure for Single-Molecule Analysis of Membrane Proteins in Whole Cells Using Electron Microscopy. *ACS Nano* **2017**, *11* (11), 11108−11117.
(59) Mohanty, N.; Fahrenholtz, M.; Nagaraja, A.; Boyle, D.; Berry, V. Impermeable Graphenic Encasement of Bacteria. *Nano Lett.* **2011**, *11* (3), 1270−1275.
(60) Peckys, D. B.; de Jonge, N. Liquid Scanning Transmission Electron Microscopy: Imaging Protein Complexes in their Native Environment in Whole Eukaryotic Cells. *Microsc. Microanal.* **2014**, *20* (2), 346−365.
(61) Peckys, D. B.; de Jonge, N. Visualizing Gold Nanoparticle Uptake in Live Cells with Liquid Scanning Transmission Electron Microscopy. *Nano Lett.* **2011**, *11* (4), 1733−1738.
(62) Dukes, M. J.; Peckys, D. B.; de Jonge, N. Correlative Fluorescence Microscopy and Scanning Transmission Electron Microscopy of Quantum-Dot-Labeled Proteins in Whole Cells in Liquid. *ACS Nano* **2010**, *4* (7), 4110−4116.
(63) Peckys, D. B.; Veith, G. M.; Joy, D. C.; de Jonge, N. Nanoscale Imaging of Whole Cells Using a Liquid Enclosure and a Scanning Transmission Electron Microscope. *PLoS One* **2009**, *4* (12), e8214.
(64) de Jonge, N.; Peckys, D. B.; Kremers, G. J.; Piston, D. W. Electron Microscopy of Whole Cells in Liquid with Nanometer Resolution. *Proc. Natl. Acad. Sci. U. S. A.* **2009**, *106* (7), 2159−2164.
(65) Liv, N.; van Oosten Slingeland, D. S. B.; Baudoin, J.-P.; Kruit, P.; Piston, D. W.; Hoogenboom, J. P. Electron Microscopy of Living Cells During *in Situ* Fluorescence Microscopy. *ACS Nano* **2016**, *10* (1), 265−273.
(66) Hirano, K.; Kinoshita, T.; Uemura, T.; Motohashi, H.; Watanabe, Y.; Ebihara, T.; Nishiyama, H.; Sato, M.; Suga, M.; Maruyama, Y.; et al. Electron Microscopy of Primary Cell Cultures in Solution and Correlative Optical Microscopy Using ASEM. *Ultramicroscopy* **2014**, *143*, 52−66.
(67) Nishiyama, H.; Suga, M.; Ogura, T.; Maruyama, Y.; Koizumi, M.; Mio, K.; Kitamura, S.; Sato, C. Atmospheric Scanning Electron Microscope Observes Cells and Tissues in Open Medium Through Silicon Nitride Film. *J. Struct. Biol.* **2010**, *169* (3), 438−449.
(68) Ogura, T. Direct Observation of Unstained Biological Specimens in Water by the Frequency Transmission Electric-Field Method Using SEM. *PLoS One* **2014**, *9* (3), e92780.
(69) Ogura, T. Nanoscale Analysis of Unstained Biological Specimens in Water without Radiation Damage Using High-resolution Frequency Transmission Electric-field System Based on FE-SEM. *Biochem. Biophys. Res. Commun.* **2015**, *459* (3), 521−528.
(70) Okada, T.; Ogura, T. Nanoscale Imaging of Untreated Mammalian Cells in a Medium with Low Radiation Damage Using Scanning Electron-assisted Dielectric Microscopy. *Sci. Rep.* **2016**, *6*, 29169.
(71) Han, Y.; Nguyen, K. X.; Ogawa, Y.; Park, J.; Muller, D. A. Atomically Thin Graphene Windows That Enable High Contrast Electron Microscopy without a Specimen Vacuum Chamber. *Nano Lett.* **2016**, *16* (12), 7427−7432.
(72) Stokes, D. J. *Principles and Practice of Variable Pressure/Environmental Scanning Electron Microscopy (VP-ESEM)*; John Wiley & Sons, Ltd.: Chichester, 2008.
(73) ESEM Home Page − ESEM Science and Technology. www.danilatos.com (accessed 2021-08-27); see also references therein.
(74) Donald, A. M. The Use of Environmental Scanning Electron Microscopy for Imaging Wet and Insulating Materials. *Nat. Mater.* **2003**, *2* (8), 511−516.
(75) Bogner, A.; Thollet, G.; Basset, D.; Jouneau, P. H.; Gauthier, C. Wet STEM: A New Development in Environmental SEM for Imaging Nano-Objects Included in a Liquid Phase. *Ultramicroscopy* **2005**, *104* (3−4), 290−301.
(76) Bogner, A.; Jouneau, P. H.; Thollet, G.; Basset, D.; Gauthier, C. A History of Scanning Electron Microscopy Developments: Towards "Wet-STEM" Imaging. *Micron* **2007**, *38* (4), 390−401.
(77) Jornsanoh, P.; Thollet, G.; Ferreira, J.; Masenelli-Varlot, K.; Gauthier, C.; Bogner, A. Electron Tomography Combining ESEM and STEM: A New 3D Imaging Technique. *Ultramicroscopy* **2011**, *111* (8), 1247−1254.
(78) Grzelak, D.; Szustakiewicz, P.; Tollan, C.; Raj, S.; Král, P.; Lewandowski, W.; Liz-Marzán, L. M. *In Situ* Tracking of Colloidally Stable and Ordered Assemblies of Gold Nanorods. *J. Am. Chem. Soc.* **2020**, *142* (44), 18814−18825.
(79) Kunstmann-Olsen, C.; Belić, D.; Bradley, D. F.; Grzelczak, M. P.; Brust, M. Humidity-Dependent Reversible Transitions in Gold Nanoparticle Superlattices. *Chem. Mater.* **2016**, *28* (9), 2970−2980.
(80) Kunstmann-Olsen, C.; Belic, D.; Brust, M. Monitoring Pattern Formation in Drying and Wetting Dispersions of Gold Nanoparticles by ESEM. *Faraday Discuss.* **2015**, *181*, 281−298.
(81) Novotný, F.; Wandrol, P.; Proška, J.; Šlouf, M. *In Situ* WetSTEM Observation of Gold Nanorod Self-Assembly Dynamics in a Drying Colloidal Droplet. *Microsc. Microanal.* **2014**, *20* (2), 385−393.
(82) Maraloiu, V. A.; Hamoudeh, M.; Fessi, H.; Blanchin, M. G. Study of Magnetic Nanovectors by Wet-STEM, a New ESEM Mode in Transmission. *J. Colloid Interface Sci.* **2010**, *352* (2), 386−392.
(83) Šlouf, M.; Lapčíková, M.; Štěpánek, M. Imaging of Block Copolymer Vesicles in Solvated State by Wet Scanning Transmission Electron Microscopy. *Eur. Polym. J.* **2011**, *47* (6), 1273−1278.
(84) Xiao, J.; Foray, G.; Masenelli-Varlot, K. Analysis of Liquid Suspensions Using Scanning Electron Microscopy in Transmission: Estimation of the Water Film Thickness Using Monte−Carlo Simulations. *J. Microsc.* **2018**, *269* (2), 151−160.
(85) Gonzalez, E.; Tollan, C.; Chuvilin, A.; Barandiaran, M. J.; Paulis, M. Determination of the Coalescence Temperature of Latexes by Environmental Scanning Electron Microscopy. *ACS Appl. Mater. Interfaces* **2012**, *4* (8), 4276−4282.
(86) Stokes, D. J.; Thiel, B. L.; Donald, A. M. Direct Observation of Water−Oil Emulsion Systems in the Liquid State by Environmental Scanning Electron Microscopy. *Langmuir* **1998**, *14* (16), 4402−4408.
(87) Kirk, S. E.; Skepper, J. N.; Donald, A. M. Application of Environmental Scanning Electron Microscopy to Determine Biological Surface Structure. *J. Microsc.* **2009**, *233* (2), 205−224.
(88) Uroukov, I. S.; Patton, D. Examination of the Transition of Cultured Neuronal Cells From Submerged to Exposed Using an Environmental Scanning Electron Microscope (ESEM). *Micron* **2014**, *56*, 1−7.
(89) Neděla, V. Controlled Dehydration of a Biological Sample Using an Alternative Form of Environmental SEM. *J. Microsc.* **2010**, *237* (1), 7−11.
(90) Ren, Y.; Donald, A. M.; Zhang, Z. Investigation of the Morphology, Viability and Mechanical Properties of Yeast Cells in Environmental SEM. *Scanning* **2008**, *30* (6), 435−442.
(91) Muscariello, L.; Rosso, F.; Marino, G.; Giordano, A.; Barbarisi, M.; Cafiero, G.; Barbarisi, A. A Critical Overview of ESEM Applications in the Biological Field. *J. Cell. Physiol.* **2005**, *205* (3), 328−334.
(92) Stokes, D. J.; Rea, S. M.; Best, S. M.; Bonfield, W. Electron Microscopy of Mammalian Cells in the Absence of Fixing, Freezing, Dehydration, or Specimen Coating. *Scanning* **2003**, *25* (4), 181−184.
(93) Zheng, T.; Waldron, K. W.; Donald, A. M. Investigation of Viability of Plant Tissue in the Environmental Scanning Electron Microscopy. *Planta* **2009**, *230* (6), 1105−1113.

https://doi.org/10.1021/acs.jpcc.1c09104
J. Phys. Chem. C XXXX, XXX, XXX−XXX

(94) Stokes, D. J.; Rea, S. M.; Porter, A. E.; Best, S. M.; Bonfield, W. Characterisation of Biomedical Materials, Cells & Interfaces Using Environmental SEM (ESEM). *MRS Proc.* **2001**, *711*, 6.
(95) McGregor, J. E.; Donald, A. M. ESEM Imaging of Dynamic Biological Processes: The Closure of Stomatal Pores. *J. Microsc.* **2009**, *239* (2), 135−141.
(96) Hermannsdörfer, J.; Tinnemann, V.; Peckys, D. B.; de Jonge, N. The Effect of Electron Beam Irradiation in Environmental Scanning Transmission Electron Microscopy of Whole Cells in Liquid. *Microsc. Microanal.* **2016**, *22* (3), 656−665.
(97) Peckys, D. B.; de Jonge, N. Gold Nanoparticle Uptake in Whole Cells in Liquid Examined by Environmental Scanning Electron Microscopy. *Microsc. Microanal.* **2014**, *20* (1), 189−197.
(98) Peckys, D. B.; Baudoin, J.-P.; Eder, M.; Werner, U.; de Jonge, N. Epidermal Growth Factor Receptor Subunit Locations Determined in Hydrated Cells with Environmental Scanning Electron Microscopy. *Sci. Rep.* **2013**, *3*, 2626.
(99) Staniewicz, L.; Donald, A. M.; Stokes, D. J.; Thomson, N.; Sivaniah, E.; Grant, A.; Bulmer, D.; Khan, A. The Application of STEM and *in Situ* Controlled Dehydration to Bacterial Systems Using ESEM. *Scanning* **2012**, *34* (4), 237−246.
(100) Thomson, N. M.; Channon, K.; Mokhtar, N. A.; Staniewicz, L.; Rai, R.; Roy, I.; Sato, S.; Tsuge, T.; Donald, A. M.; Summers, D.; et al. Imaging Internal Features of Whole, Unfixed Bacteria. *Scanning* **2011**, *33* (2), 59−68.
(101) Cismak, A.; Schwanecke, M.; Füting, M.; Heilmann, A. Environmental Scanning Electron Microscopy of Living Mammalian Cell Cultures. *Microsc. Microanal.* **2003**, *9*, 480−481.
(102) Neděla, V.; Tihlaříková, E.; Maxa, J.; Imrichová, K.; Bučko, M.; Gemeiner, P. Simulation-Based Optimisation of Thermodynamic Conditions in the ESEM for Dynamical *in Situ* Study of Spherical Polyelectrolyte Complex Particles in Their Native State. *Ultramicroscopy* **2020**, *211*, 112954.
(103) Lundberg, M.; Johansson, M. Positively Charged DNA-Binding Proteins Cause Apparent Cell Membrane Translocation. *Biochem. Biophys. Res. Commun.* **2002**, *291* (2), 367−371.
(104) Danilatos, G. D. Foundations of Environmental Scanning Electron Microscopy. *Adv. Electron. Electron Phys.* **1988**, *71*, 109−250.
(105) Cameron, R. E.; Donald, A. M. Minimizing Sample Evaporation in the Environmental Scanning Electron Microscope. *J. Microsc.* **1994**, *173* (3), 227−237.
(106) Leary, R.; Brydson, R. Characterisation of ESEM Conditions for Specimen Hydration Control. *J. Phys. Conf. Ser.* **2010**, *241* (1), 012024.
(107) McGregor, J. E.; Staniewicz, L. T. L.; Guthrie, S. E.; Donald, A. M. Environmental Scanning Electron Microscopy in Cell Biology. In *Cell Imaging Techniques*; Taatjes, D. J., Roth, J., Eds.; Methods in Molecular Biology; Humana Press: Totowa, NJ, 2013; pp 493−516.
(108) de Jonge, N.; Pfaff, M.; Peckys, D. B. Practical Aspects of Transmission Electron Microscopy in Liquid. *Adv. Imaging Electron Phys.* **2014**, *186*, 1−37.
(109) Nikoobakht, B.; El-Sayed, M. A. Preparation and Growth Mechanism of Gold Nanorods (NRs) Using Seed-Mediated Growth Method. *Chem. Mater.* **2003**, *15* (10), 1957−1962.
(110) Faria, M.; Björnmalm, M.; Thurecht, K. J.; Kent, S. J.; Parton, R. G.; Kavallaris, M.; Johnston, A. P. R.; Gooding, J. J.; Corrie, S. R.; Boyd, B. J.; et al. Minimum Information Reporting in Bio−Nano Experimental Literature. *Nat. Nanotechnol.* **2018**, *13* (9), 777−785.
(111) Faria, M.; Björnmalm, M.; Crampin, E. J.; Caruso, F. A Few Clarifications on MIRIBEL. *Nat. Nanotechnol.* **2020**, *15* (1), 2−3.
(112) Vivès, E.; Brodin, P.; Lebleu, B. A Truncated HIV-1 Tat Protein Basic Domain Rapidly Translocates through the Plasma Membrane and Accumulates in the Cell Nucleus. *J. Biol. Chem.* **1997**, *272* (25), 16010−16017.
(113) Lévy, R.; Thanh, N. T. K.; Doty, R. C.; Hussain, I.; Nichols, R. J.; Schiffrin, D. J.; Brust, M.; Fernig, D. G. Rational and Combinatorial Design of Peptide Capping Ligands for Gold Nanoparticles. *J. Am. Chem. Soc.* **2004**, *126* (32), 10076−10084.
(114) Royall, C. P.; Thiel, B. L.; Donald, A. M. Radiation Damage of Water in Environmental Scanning Electron Microscopy. *J. Microsc.* **2001**, *204* (3), 185−195.
(115) Woehl, T. J.; Jungjohann, K. L.; Evans, J. E.; Arslan, I.; Ristenpart, W. D.; Browning, N. D. Experimental Procedures to Mitigate Electron Beam Induced Artifacts during *in Situ* Fluid Imaging of Nanomaterials. *Ultramicroscopy* **2013**, *127*, 53−63.
(116) Schneider, N. M.; Norton, M. M.; Mendel, B. J.; Grogan, J. M.; Ross, F. M.; Bau, H. H. Electron−Water Interactions and Implications for Liquid Cell Electron Microscopy. *J. Phys. Chem. C* **2014**, *118* (38), 22373−22382.
(117) Grogan, J. M.; Schneider, N. M.; Ross, F. M.; Bau, H. H. Bubble and Pattern Formation in Liquid Induced by an Electron Beam. *Nano Lett.* **2014**, *14* (1), 359−364.
(118) Woehl, T. J.; Abellan, P. Defining the Radiation Chemistry during Liquid Cell Electron Microscopy to Enable Visualization of Nanomaterial Growth and Degradation Dynamics. *J. Microsc.* **2017**, *265* (2), 135−147.
(119) Egerton, R. F. Control of Radiation Damage in the TEM. *Ultramicroscopy* **2013**, *127*, 100−108.
(120) Kennedy, E.; Nelson, E. M.; Tanaka, T.; Damiano, J.; Timp, G. Live Bacterial Physiology Visualized with 5 nm Resolution Using Scanning Transmission Electron Microscopy. *ACS Nano* **2016**, *10* (2), 2669−2677.
(121) de Jonge, N.; Peckys, D. B. Live Cell Electron Microscopy Is Probably Impossible. *ACS Nano* **2016**, *10* (10), 9061−9063.
(122) Kennedy, E.; Nelson, E. M.; Damiano, J.; Timp, G. Gene Expression in Electron-Beam-Irradiated Bacteria in Reply to "Live Cell Electron Microscopy Is Probably Impossible". *ACS Nano* **2017**, *11* (1), 3−7.
(123) de Jonge, N. Theory of the Spatial Resolution of (Scanning) Transmission Electron Microscopy in Liquid Water or Ice Layers. *Ultramicroscopy* **2018**, *187*, 113−125.
(124) de Jonge, N.; Poirier-Demers, N.; Demers, H.; Peckys, D. B.; Drouin, D. Nanometer-Resolution Electron Microscopy Through Micrometers-thick Water Layers. *Ultramicroscopy* **2010**, *110*, 1114−1119.
(125) Woehl, T.; Keller, R. Dark-field Image Contrast in Transmission Scanning Electron Microscopy: Effects of Substrate Thickness and Detector Collection Angle. *Ultramicroscopy* **2016**, *171*, 166−176.

https://doi.org/10.1021/acs.jpcc.1c09104
J. Phys. Chem. C XXXX, XXX, XXX−XXX